Low-Energy Electron Collisions With Multiply-Charged Positive Ions

A. Chutjian, J. B. Greenwood and S. J. Smith

Jet Propulsion Laboratory, California Institute of Technology
Pasadena, CA 91109 USA

Abstract. Cross sections for a variety of electron-ion collision phenomena are the backbone for understanding energy balance in high electron temperature plasmas. Such plasmas include such seemingly disparate objects such as the Io torus around Jupiter, solar and stellar atmospheres, the interstellar medium, and fusion devices. Several experimental approaches used with multiply-charged ions (MCIs) will be reviewed. These include measurement of excitation cross sections using the electron energy-loss method, measurement of ionic lifetimes using a Kingdon trap, and measurement of dissociative recombination cross sections using ion storage rings. New JPL results will be presented of e-S^{2+} inelastic scattering, relevant to the problem of ion density and radiated energy in the Io torus; and metastable-state lifetimes in C^+, N^+, and Ar^{2+} relevant to stellar absorption by the interstellar medium.

INTRODUCTION

Electron-ion interactions are present in a variety of astronomical objects such as the sun, stars, quasars, planetary nebulae, the interstellar medium, comets, planetary magnetospheres and ionospheres. The electron energies and ionic charge states will depend on the object: a violent solar flare can produce emissions in Fe^{24+} (IP of 8828 eV), while a dense interstellar cloud can have a high density of co-existent singly-charged atomic and molecular ions, and thermal electrons as cold as 10-100 K.

Excitation cross sections are needed to convert, for example, the rich optical emissions observed by the Hubble Space Telescope (especially from the GHRS and STIS instruments), the Extreme Ultraviolet Explorer, and from the many ground-based telescopes, into ion densities. In the equations of statistical equilibrium the collision strength and the radiative emission rate play key roles in determining an excited-state ion population (1). In the simple case of coronal equilibrium one has the expression useful in determining the electron temperature T_e for the excited-state population N_i,

$$N_i = N_e N_g C(g \to i)/A(i \to g) \qquad (1)$$

where g refers to the ion ground state, and $C(g \rightarrow l)$, $A(l \rightarrow g)$ are the collisional excitation rate (cm^3/sec) and the spontaneous radiative decay rate (sec^{-1}), respectively. The collision rate is an average of the collision strength or cross section over the (usually) Maxwellian electron distribution function of the astronomical plasma described by T_e. Low-energy electron excitation cross sections are difficult to calculate, and any calculation has to be benchmarked against reliable measurements. As evident from Eq. (1) Einstein A-values are also required in large numbers. The majority have to be calculated, but a smaller fraction need to be measured experimentally in order to calibrate theory.

Finally, the broader issue of ionization equilibrium in hot solar, stellar, and fusion plasmas involves phenomena such as direct and dielectronic recombination; photoionization, electron ionization (both direct and indirect); and charge exchange (1). A vast array of theoretical and experimental cross sections, with and without superimposed electric fields (critical in the case of dielectronic recombination) are required.

THE ELECTRON ENERGY-LOSS METHOD

The electron energy-loss method, when applied to singly- and multiply-charged ion targets, can provide a more versatile path for exciting spin- and symmetry-forbidden transitions than can, for example, excitation-optical emission methods. The process can be represented as,

$$e(E,0^\circ) + A(nl)^{m+} \rightarrow e(E-\Delta E,\theta) + A(n'l') \qquad (2)$$

where ΔE is the electron energy loss corresponding to the energy difference between the nl and $n'l'$ states, and θ is the electron polar scattering angle. As seen in Eq. (2), one is able to measure *angular distributions* of elastically- and inelastically-scattered electrons. These differential cross sections (DCSs) provide a more stringent test of theory, since the angular results probe both the short-range (large scattering angles) and long-range (small scattering angles) portions of the e-ion scattering potential. Calculated integral cross sections, while the preferred input to plasma-modeling calculations, tend to integrate over approximations to the scattering potential, wavefunction, number of states, *etc.*

Recent methods applied to energy-loss scattering can be divided into those using crossed electron-ion beams (3,4) and merged beams (5,6). Crossed beams have been

used to measure elastic, superelastic, and inelastic DCSs, and merged beams to detect inelastically-scattered electrons collected over the angular range $\{0,\pi\}$. Representative results for both classes of experiments will be reviewed in the following two sections.

Inelastic Scattering

The first application of energy-loss techniques to ions was in a crossed-beams geometry (7). A highly-collimated, non-monochromatized incident electron beam was used, with a 180° hemispherical analyzer for electron energy analysis. The resonance $4^2S \rightarrow 4^2P$ in Zn^+ was detected, and relative DCS with comparison to a five-state close-coupling theory, reported (8). Further DCS were obtained on low-lying allowed and forbidden transitions in Mg^+, Zn^+, and Cd^+ (9).

As mentioned above, the primary need in both astronomical and fusion plasmas is the *integral* excitation cross section (10). Two similar methods of approach have been developed, at JPL (5,11-13) and at ORNL (6,14-16), using energy-loss and merged-beams methods. In these approaches, one is able to handle issues of full angular collection, good signal-to-backgrounds, efficient electron detection, and be able to accommodate MCIs as the target.

Details of the ORNL apparatus are given by Bannister, *et al.* in this volume. A brief description will be given here of the JPL apparatus, with an indication of differences between the JPL and ORNL methods. Shown in Fig. 1 is a schematic of the JPL MCI facility (13). The facility is designed to generate high charge states using the *Caprice* 14 GHz electron-cyclotron resonance ion source. Separate beam lines are dedicated to measuring excitation cross sections in a merged-beams section, ion lifetimes in a Kingdon-trap section, and charge-exchange cross sections with a neutral gas cell. Recent additions to the merged-beams sections are a multipole "electronic aperture" **EA** to separate elastically-scattered electrons, with their larger gyroradii, from the inelastically-scattered electrons (17); a new vane system with finer sampling of the electron and ion beam profiles; and a new beam-pulsing unit using fast MOSFET switches (18), with PC control of all pulsing, beams-profile monitoring, and data acquisition. Some differences between the JPL and ORNL merged-beams system are: (a) metallic beam profile monitors to monitor profiles at four locations in a 21.0 ± 0.3 cm merged pathlength (microchannelplate-CCD camera combination for ORNL which monitors continuously along a 6.35 cm pathlength), (b) location of a PSD along the magnetic-field direction (orthogonal in the ORNL setup) allowing discrimination against energetic electrons using retarding grids, an electron mirror MI to reflect into the forward PSD electrons which are backscattered ($\vartheta > 90°$) in the LAB frame, (d) an electronically-variable multipole aperture (five physical apertures in the ORNL system)

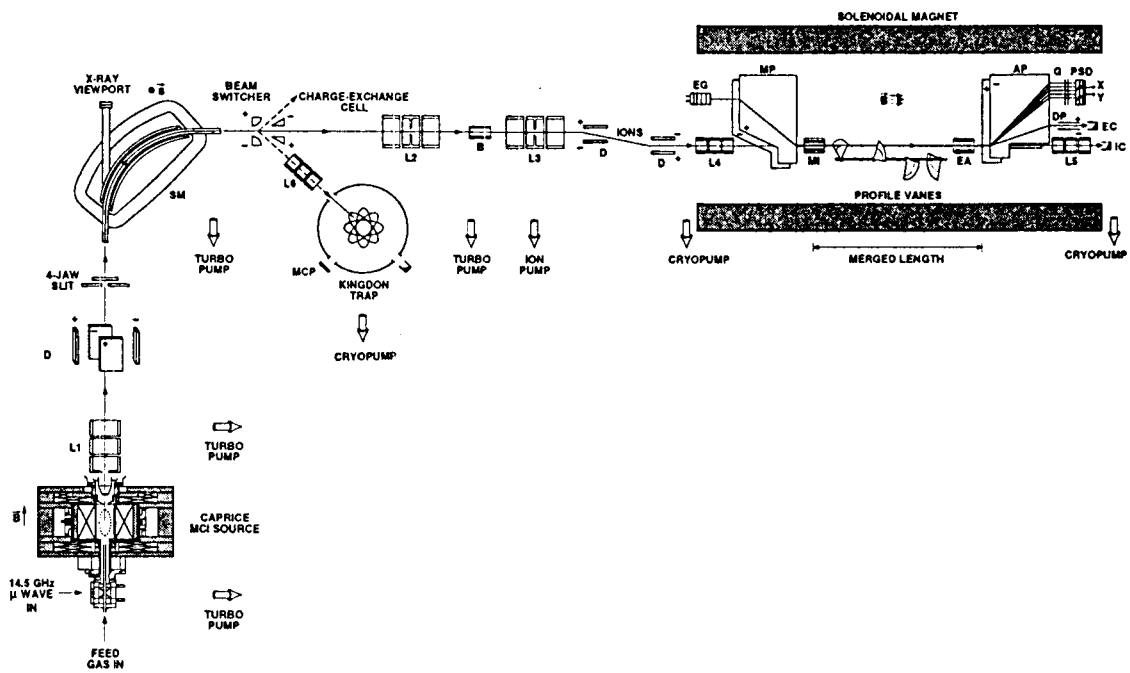

FIGURE 1. Present configuration of the JPL multiply-charged ion facility. **(L1-L5)**, three-element focusing lenses, **(B)** differential pumping baffle, **(D)** deflector plates, **(MP)** merging trochoidal plates, **(AP)** analyzing trochoidal plates, **(MI)** electron mirror, **(EA)** electronic aperture, **(DP)** trochoidal deflection plates to deflect parent electron beam out of the scattering plane, **(PSD)** position-sensitive detector.

to filter unwanted elastically-scattered electrons having the same axial velocity as inelastically-scattered electrons.

As is well known, ion beams produced in discharges can contain a significant fraction *f* of metastable states. The population of these states will depend on lifetime, ion transit time from source to target, and the source operating conditions (microwave power, gas pressure, *etc.*). The presence of metastables means that only a fraction *(1-f)* of the total beam current is available for excitation, while the entire beam is counted in measurement of the ion current. Hence any measured cross section will be smaller than its true value by a factor *1/(1-f)*. In the JPL approach an ion-beam attenuation method is used, wherein a section of the beam line is filled with a charge-exchange (*ce*) gas (He, N_2, or Ar). Assuming that different excited states will have a different *ce* cross section, one will observe breaks in the slope of the transmitted current *vs* pressure. Extrapolation of the high-pressure slope (corresponding to *ce* by the ground state) to zero pressure will

give the metastable fraction. Fractions as high as 75% have thus far been observed in the JPL *Caprice* source. (Interestingly, one would like to *minimize f* for the excitation measurements, and *maximize f* for metastable *f*-value measurements! See below.)

Shown in Figs. 2 and 3 are several recent JPL results on excitation of singly-charged C^+ (5) and S^+ (12). These ions are strong emitters in solar and stellar atmospheres, and in the Io torus (S^+). It is interesting to note that the torus is supplied by SO_2 from volcanic action on Io (19). The SO_2 is dissociated and ionized by the energetic particle environment at Jupiter, and ions are trapped in Jupiter's magnetosphere. Successive ionizations of the trapped singly-charged ions lead to higher charge states of *S* and *O*. Shown In Fig. 4 are the first JPL results in MCIs, in this case excitation of the $3s^23p^2\ ^3P \rightarrow 3s3p^3\ ^5S^\circ$ transition in e-S^{2+} (20). Comparison with a 17-state close-coupling calculation (21) shows good agreement between experiment and theory, especially for the broad resonances at 11.5 eV. It is essential to filter out as completely as possible the elastically-scattered electrons. A schematic of the so-called electronic aperture, used in the results of Fig. 5 to eject the unwanted elastically-scattered electrons, is shown in Fig. 5. It consists of sixteen 2.00-mm dia rods, each 25.0 mm long. Potentials of equal and opposite sign are impressed on the rods, forming a null potential in the center of the structure through which the merged electron and ion beams

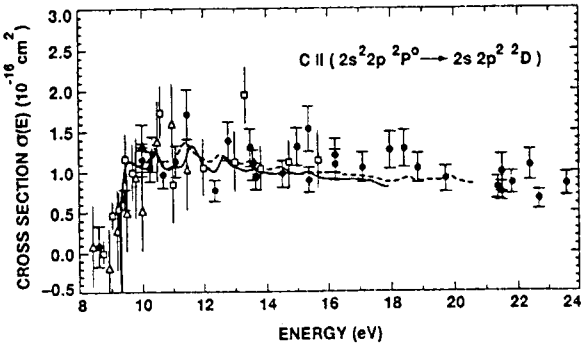

FIGURE 2. Experimental (filled circles) and an 8-state *R*-matrix cross sections (solid line, convoluted with a 250 meV FWHM resolution) in C^+ (5). Other data: Luo and Pradhan (22) theory (dashed line), Lafyatis and Kohl experiment (open square)(23), and Greenwood *et al.* experiment (open triangle)(24).

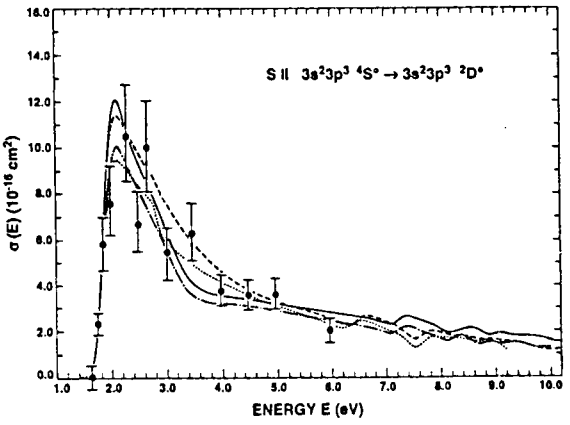

FIGURE 3. Experimental (filled circles) and 19-state close-coupling cross sections (solid line, convoluted with a 250 meV FWHM resolution) in S^+ (12). Other theories: 19-state *R*-matrix [dash-dot line (25)], 12-state *R*-matrix [dashed line (26)], 6-state *R*-matrix [dotted line (27)].

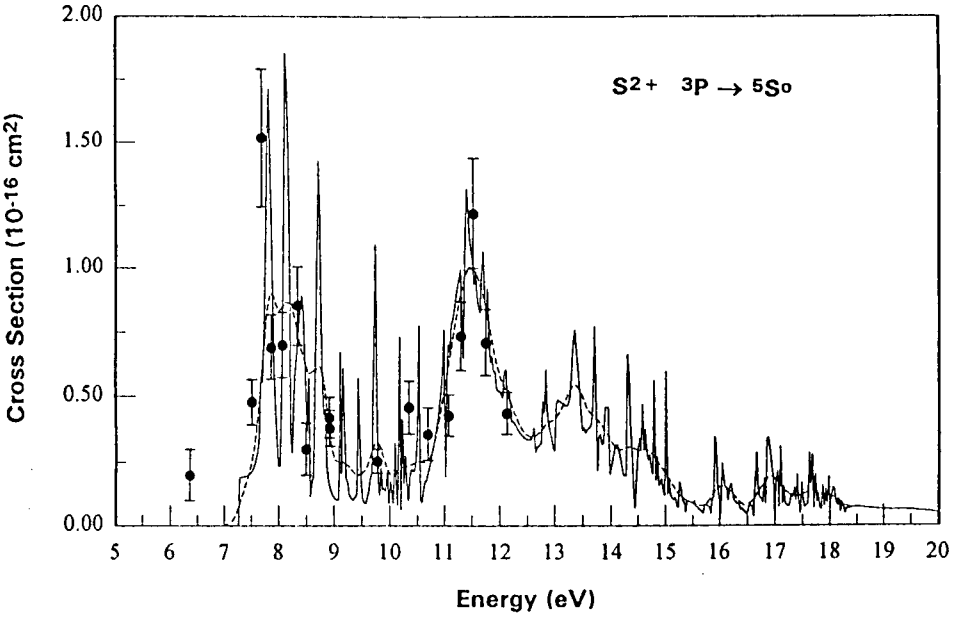

FIGURE 4. Experimental (filled circles) (20) and theoretical cross sections [solid line (21)] for the $3s^2 3p^2\ ^3P \rightarrow 3s3p^3\ ^5S^\circ$ transition in S^{2+}. Dashed line is theory line convoluted with a 250 meV FWHM resolution.

pass. An elastically-scattered electron with its larger gyroradius will make an excursion close to the poles and be ejected into the shield. An inelastically-scattered electron with its smaller perpendicular energy will stay closer to the null center and traverse the aperture. The diameter of the "iris" of the aperture is set by the potentials of the rods. Further details will be presented elsewhere (19).

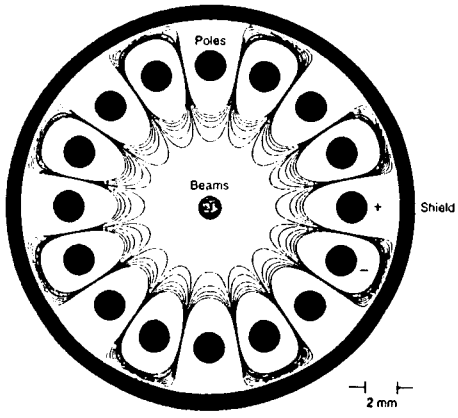

FIGURE 5. Schematic of an "electronic aperture" used to filter elastically-scattered electrons with their larger gyroradii (19). This end-on view shows sixteen rods symmetrically placed about the merged beams axis (shaded central region). Opposite potentials are placed on adjacent rods, and unwanted electrons are ejected into the positively-biased shield.

Elastic Scattering

It has been noted in the previous section that elastic scattering can be an unwelcome addition to electron-ion excitation signal. For typical collision energies the elastic scattering signal can be order of magnitude greater than the inelastic signal, especially for high charge states. Although various techniques are applied to remove this corrupting signal an estimate of the elastic contribution may be necessary. For this reliable elastic differential and integral cross sections are required.

In plasmas elastic electron-ion scattering determines properties such as electron transport coefficients and ion heating rates. In modeling these parameters the classical Rutherford Coulomb DCS is often used. This DCS is strongly forward peaked. However Greenwood and Williams (28) have demonstrated deviations from the Coulombic formula which can have significant effect on the momentum-transfer cross section for certain types of plasmas. Therefore, the accurate angular distribution has to be taken into account to obtain an accurate plasma model.

Elastic scattering from a Coulombic potential can be solved analytically (29), and the result is equivalent to the classical Rutherford scattering model,

$$\frac{d\sigma}{d\Omega} = \frac{q^2}{16E^2\sin^4(\theta/2)} , \qquad (3)$$

where $d\sigma/d\Omega$ is the elastic DCS, E the electron energy, q the ionic charge, and θ the scattering angle. For partially-stripped ions the scattering potential is only Coulombic for large distance, so the potential can be written as $V = V_C + V_S$, where V_C is the Coulombic (long-range) potential and V_S is the short-range potential. Similarly, the scattering amplitude may be represented as a Coulombic and a short-range part (29) by $f = f_C + f_S$, to give a DCS as,

$$\frac{d\sigma}{d\Omega} = |f_C|^2 + |f_S| + 2Re[f_C^* f_S] .$$

This formula indicates that there is a Coulombic contribution to the DCS, a short-range part, and an interference term, respectively. The interference term can give dramatic deviations from the usual Coulomb formula in Eq. (3), especially at large scattering angles where the long range contribution is weak. Examples of this interference can be seen in recent elastic DCS measurements, shown here in Fig. 6 (4).

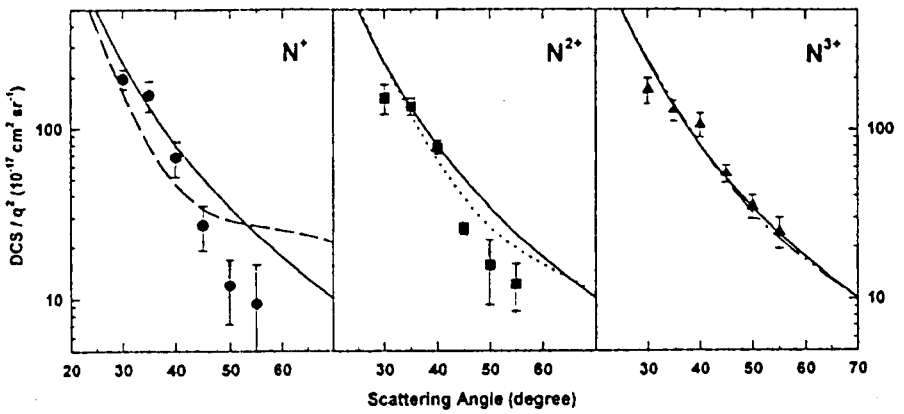

FIGURE 6. DCS, reduced by q^2, for elastic electron scattering from N^{q+} (q = 1-3) at 10 eV (4). Solid line in each case is the Rutherford formula [Eq.(3)], and broken lines are from Ref. 31.

The scattering amplitudes can be determined by calculating the Coulomb and short-range phase shifts. The former are given by gamma functions, and the latter can be calculated numerically given an assumed form for V_S. Manson (30) and Szydlik *et al.* (31) have done so for singly-charged ions, and some MCIs. A database of short-range phase shifts for all ions has recently been completed (32).

Elastic scattering was first investigated by an indirect method of fast ion-atom scattering through analysis of scattered binary-encounter electrons. Electrons scattered at $\vartheta = 0°$ in the LAB frame correspond to $\theta = 180°$ scattering in the projectile frame. Larger LAB angles correspond to smaller CM angles. Energy broadening of the emitted electron spectra occurs because the electrons are not stationary in the atom, but have a characteristic momentum distribution, the Compton profile. To assess the experimental data it is necessary to fold this profile into theoretical results. However, this limits the usefulness of the technique to large electron-ion scattering energies (E > 100 eV). A summary of experimental and theoretical investigations of binary-encounter electrons has been given by Liao *et al.* (33). Large enhancements in the DCS at $\theta = 180°$ have been observed. These increase with lower charge states of the partially-stripped ions, in contradiction to the Rutherford formula. Indications of interference structure in the DCS appear in some angular measurements, best shown in Ref. 34.

Due to the inherently difficult nature of electron-ion scattering measurements (low ion densities, requiring ultrahigh vacuum techniques and beams modulation) there are few direct scattering measurements, but the existence of interference structure in the DCS provides a sensitive test of theory. Basically, the interference is due to close-in (low partial waves) electron-ion interactions, where the electron can better "feel" the

details of the (non-Coulomb) ion scattering potential. Agreement between experimental measurements (3,30,34-38) and partial-wave calculations (3,30-32,35) has been reasonably good. However, Srigengan *et al.* (39) find poorer agreement in energy-dependent measurements at fixed scattering angles. Other differences occur in the more sophisticated many-body perturbation theory (32), which is in accord with measurements of Huber *et al.*, but not with Srigengan *et al.* (38). Possible effects of polarization at large scattering angles has been suggested (40,41), but *R*-matrix calculations (42) with and without polarized pseudostates indicate that this is not a significant effect for the case of Ar^+.

These diverse results indicate that further e-ion elastic DCS measurements are required, especially at large scattering angles. Deviations from the Rutherford formula are dramatic, even for highly-charged ions. For plasma modeling the use of the short-range phase shifts of Manson and Turner to calculate DCSs is recommended.

MEASUREMENTS OF LIFETIMES AND f-VALUES

Because of the high sensitivity and optical resolution of present and planned space missions weak absorption and emissions, previously undetected, now assume new importance. One example is detection in the long path length through the interstellar medium (ISM) of weak spin- and symmetry-forbidden transitions from metastable levels in singly- and multiply-charged positive ions (43-45). Strong electric-dipole transitions lead to absorption lines in the ISM with equivalent widths (EW) that lie on the saturated part of the curve of growth. Hence reliable column densities require transitions (metastable) with small *f*-values, where EW's now lie on the linear part of the curve. Because rates for collisional excitation and de-excitation of ions in diffuse plasmas are comparable to radiative decay rates from metastable levels, the intensity ratios between forbidden and allowed transitions are density- and temperature sensitive (46) and critically depend on the lifetimes of the metastable or intersystem line (47,48). However, calculated and measured lifetimes in some cases can differ by a factor of three.

Use of the Kingdon Trap for Metastable Lifetime Measurements

For measuring the long radiative lifetimes of metastable states, long storage times are required: hence the use of an ion trap under ultrahigh vacuum operation for minimizing collisional de-excitation effects. One can store the ions, and access prominent intersystem and forbidden decays (45). Decay channels include intercombination, electric quadrupole E2, magnetic dipole M1 and double photon decay 2E transitions. The use of a Kingdon trap was first reported by Prior (49), and a number of lifetime measurements using it have

been reported by Smith, Parkinson, and co-workers (46,50-55). Lifetime measurements have been made for C^{2+} 190.9 nm (46), and O^{2+} 166.1, 166.6 nm (54). Kingdon traps have been used to measure lifetimes of Ar^{2+}, $Kr^{2+,3+}$, $Xe^{2+,3+}$, B^{+} , N^{+}, and Cu^{+} (49,56). Lifetime measurements carried out in Paul, Penning and Kingdon ion traps have been reviewed through 1993 (56).

The lifetime measurements in metastable MCIs reported herein use the JPL *Caprice* electron-cyclotron resonance ion source (Fig. 1). The metastable population in the beam is measured by filling a gas cell region with a charge exchanging gas such as Ar, N_2 or He and monitoring the fraction of transmitted ion beam *vs* target gas pressure. Populations can range from 25% to 75% of the total beam current, depending on ion charge state and operating parameters of the source such as gas pressure and microwave power.

The mean lifetime of an upper level k is related to the transition rates or decay rates A_{jk} to N lower levels I the by,

$$\tau_k^{-1} = \sum_{i=1}^{N} A_{ik} \, . \qquad (4)$$

The oscillator strength f_{ik} and the A-value are connected *via* the standard expression,

$$A_{ki}(\mathrm{sec}^{-1}) = \frac{6.670 \times 10^{13}}{\lambda^2} \frac{g_i}{g_k} f_{ik} \, . \qquad (5)$$

Here g_i and g_k are the statistical weights of levels I and k, and λ is in nanometer. It is apparent from Eqs. (4) and (5) that when there is only one channel branch for the decay of the metastable state, the lifetime yields the A-value or f-value of the transition directly. When more than one decay channel is open, the branching ratios of the transitions must be known (experimentally or theoretically) in order to obtain individual A- or f- values. The JPL ion trap, constructed in collaboration with Texas A & M University (57) is on a dedicated beam line. In the Kingdon ion trap ions are launched into orbits of defined angular momentum about a charged electrode (wire) which is pulsed once during the trapping cycle. The trap is formed by two coaxial cylinders, terminated at each end by cap electrodes. The ion trap is 15 cm long and 10 cm diameter. Four 2-cm dia apertures gird the middle of the cylinder. One aperture is for the ion beam entrance, one for the beam exit into its Faraday cup, one is for the UV fluorescence-detection optics, and one for dumping the trap contents onto an ion-counting CEM detector. The UV photon emissions are detected by an interference filter and phototube using a UV grade quartz optical system. For transitions shorter than 180 nm a UV-enhanced, CsI-coated CEM is used. A cryopump provides residual gas pressures in the vacuum chamber on the order 8×10^{-10} torr.

A multichannel analyzer records the decay N(t) of the upper state as

$$N(t) = N_o \exp[-t/\tau_m] + B. \quad (6)$$

where τ_m is the measured lifetime and B is a background term. The measured decay rate τ_m^{-1} is the sum of two rates,

$$\tau_m^{-1} = \tau^{-1} + \tau_Q^{-1} . \quad (7)$$

The quantity τ_Q^{-1} is the rate of loss of metastable ions due to collisional quenching within the trap and τ^{-1} is the natural decay rate of the metastable ion. The collisional quenching decay rate τ_Q^{-1} can be expressed as the product kn_P of the collision rate coefficient k and n_P, the density of the background gas. Experimentally, the total decay rate τ_m^{-1} is measured as a function of background pressure P at about 10 different pressures. A plot is made of τ_m^{-1} *vs* P. The intercept at zero pressure yields τ^{-1} and the slope yields k. At each P the data-taking procedure requires about 2500 scans (fill-dump cycles) and each scan last about 250-500 ms. The accuracy of the lifetimes measured are in the range 4-10% (56), which is the accuracy required by astronomers.

JPL Radiative Lifetime Measurements

Ar^{2+}: The trapping technique was first tested with the Ar^{2+} ^1S_o – $^1D_2$ transition at 519.5 nm. This transition was measured previously (57), with results comparing favorably with the available calculations (58,59). JPL preliminary results are shown in Fig. 7. The lifetime of τ= 127 ms compares with the measured results of 121.3 ms. This measured lifetime must be corrected for ion storage lifetimes, as shown in Eq.(7). Extrapolation to zero pressure resulted in a finite ion storage time constant of 511 ms for Ar^{2+}. The extrapolated lifetime is τ = 169 ms, which is good agreement with the calculated work.

C^+: Boron-like ions of carbon, nitrogen and oxygen are astrophysical-abundant and spectra are observed in a number of astronomical sources. The $2s2p^2$ ^4P – $2s^22p$ ^2P_o intersystem transitions at 232.5 nm were measured in C^+. The upper $2s2p^2$ ^4P state has three components, each decaying to the ground ^2P_o term. The emissions consist of five closely-spaced lines (60). Measurements (61) and calculations (52,63) also exist. The emission signal is seen to consist of three exponential components, corresponding to the radiative decay of the J= ½, 3/2 and 5/2 fine-structure levels. For the JPL effort, a narrow-band interference filter centered at a wavelength of 232 nm was used. Shown in Fig. 8 are preliminary C^+ results. The base pressure was 6×10^{-9} torr with the ECR beam on. Nitrogen was also deliberately added to the vacuum chamber to produce a set of plots

of decay rate *vs* N_2 pressure, with pressure ranging from (6-115)$\times 10^{-9}$ torr. The true rates were obtained by extrapolating to zero N_2 pressure.

N^+: JPL measurements were recently started on the radiative lifetime of the $2s2p^3\ ^5S_2$ metastable state of N^+. This state decays by the E1 transition $2s2p^3\ ^5S_2 \rightarrow 2s^2 2p^2\ ^3P_{0,1,2}$ at 214 nm. These emissions are readily detected in auroral spectra from satellite observations. Three theoretical studies (64-66) and three measurements (67-69) of the N^+ $^5S_2$ lifetime have been reported, hence N^+ is a good benchmark to test the JPL apparatus. One measurement (69) is 5.4 $\pm$ 0.3 ms, while the JPL preliminary lifetime is $\tau = 5.0 \pm 1.5$ ms. The final experimental error is expected to be at the 5% level.

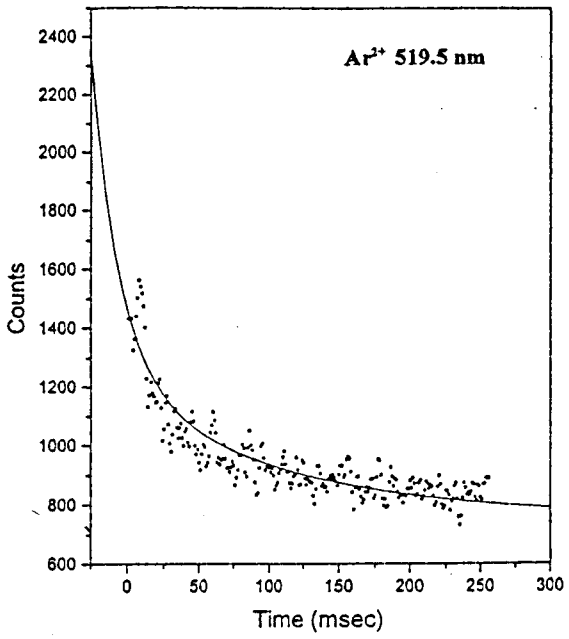

FIGURE 7. Decay of the Ar^{2+} 519.5 nm emission as function of time. Experimental data points are shown as circles and the solid line along with a two-term exponential fit shown as a solid line. The longer term measures 127 ms.

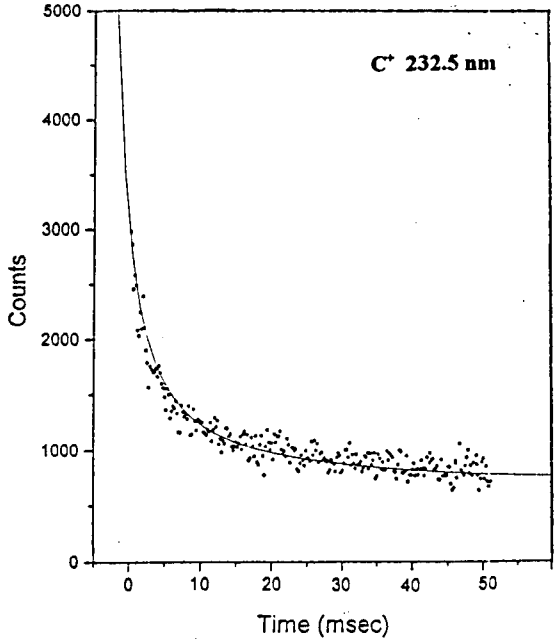

FIGURE 8. Decay of the C^+ 232.5 nm emission as a function of time at a base pressure of 6×10^{-9} torr. Experimental points are shown along with a three-term exponential fit.

ELECTRON-ION RECOMBINATION

With the use of storage rings in the various European laboratories the study of electron-atom and electron-molecular ion recombination has become a highly-developed field. A recent example of the dissociative recombination (DR) in the ions H_2O^+, H_3O^+, and CH_3^+ may be found in Vejby-Christensen *et al.*(70) using the ASTRID storage ring. With large energies in the LAB frame, CM energies in the merged cooler region as low

as 10^{-4} eV can be attained. This correspond to a lower electron temperature of about 1 K, hence data are relevant for ionization balance and molecular formation in interstellar clouds where temperatures are of the order 10-100 K. Several reviews, including that of the operation of the CRYRING, may be found in Refs. 71 and 72. Another recent example of dissociative recombination is that of e-O_2^+ recombination which is relevant to a planet within our own solar system — the earth. Shown in Fig. 9 are the projected distances for neutral atoms formed in the DR process $e + {}^{18}O^{16}O^+ \rightarrow 2O$, where the states of O can be ^{3}P, ^{1}D, or ^{1}S (73). (Long ion storage times and the use of mixed isotopes ensured that the metastable $a^4\Pi_u$ and vibrational levels had decayed.) From the product yields of Fig. 9 one finds that the total quantum yield for O(^{1}S) production is 0.05 $\pm$ 0.02, about an order of magnitude larger than the previously-assumed values of 0.0012-0.0016. This higher yield helps explain the bright emissions observed in the O(^{1}S) $\rightarrow$ O(^{3}P) 557.7 nm green line as arising from DR, without having to invoke a new source of O(^{1}S) in the atmosphere.

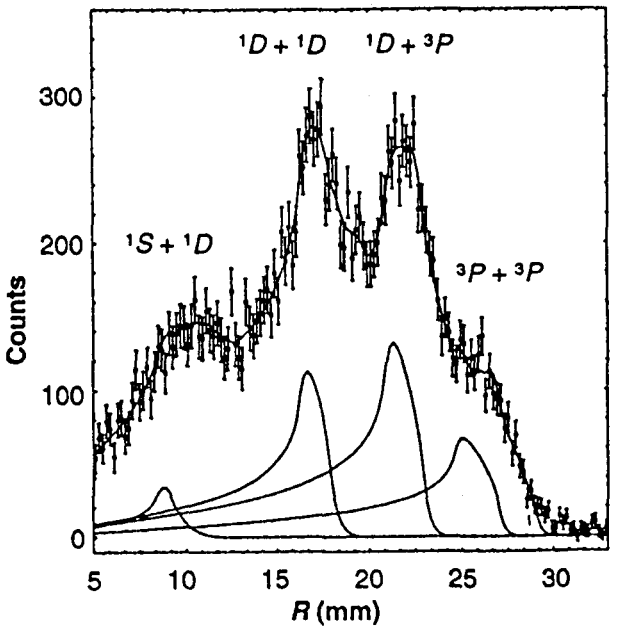

FIGURE 9. Product-state distance distribution arising from the process $e + {}^{18}O^{16}O^+ \rightarrow 2O$, with the atomic states of O as indicated (73).

ACKNOWLEDGMENTS

JBG thanks the National Research Council for a fellowship though the NASA-NRC program. This work was carried out at the Jet Propulsion Laboratory, California Institute of Technology, and was supported by the National Aeronautics and Space Administration.

REFERENCES

1. Mason, H. E., and Monsignori Fossi, B. C., *Astron. Rev.* **6**, 123-179 (1994).
2. Smith, S. J., Chutjian, A., Mitroy, J., Tayal, S. S., Henry, R. J. W., Man, K-F., Mawhorter, R. J., and Williams, I. D., *Phys. Rev. A* **48**, 292-309 (1993).
3. Belenger, C., Defrance, P., Friedlein, R., Guet, C., Jalabert, D., Maurel, M., Ristori, C., Rocco, J. C., and Huber, B. A., *J. Phys. B* **29**, 4443-56 (1996).
4. Williams, I. D., Srigengan, B., Greenwood, J. B., Newell, W. R., Platzer, A., and O'Hagan, L., *Physica Scripta* **T73**, 119-20 (1997).
5. Smith, S. J., Zuo, M., Chutjian, A., Tayal, S. S., and Williams, I. D., *Astrophys. J.* **463**, 808-17 (1996).
6. Bannister, M. E., Chung, Y.-S., Djurić, N., Wallbank, B., Woitke, O., Zhou, S., Dunn, G. H., and Smith, A. C. H., *Phys. Rev. A* **57**, 278-81, (1998).
7. Chutjian, A., and Newell, W. R., *Phys. Rev. A* **26**, 2271-3 (1982).
8. Chutjian, A., Msezane, A. Z., and Henry, R. J. W., *Phys. Rev. Letters* **50**, 1357-60 (1983).
9. Williams, I. D., Chutjian, A., and Mawhorter, R. J., *J. Phys. B* **10**, 2189-98 (1986), and refs. therein.
10. Models to date do not require knowledge of the trajectory and energy of an electron incident on a plasma. One application of DCSs would be in the earth's upper atmosphere: e-neutral DCS can give a better description of the magnetically-confined electrons raining down at the earth's poles to generate the aurora.
11. Smith, S.J., Man K-F., Mawhorter, R. J., Williams, I. D., and Chutjian, A., *Phys. Rev. Letters* **67**, 30-3 (1991).
12. Liao, C., Smith, S. J., Hitz, D., Chutjian, A., and Tayal, S. S., *Astrophys. J.* **484**, 979-84 (1997).
13. Liao, C., Smith, S. J., Chutjian, A., and Hitz, D., *Phys. Scripta* **T73** 382-3 (1997).
14. Wåhlin, E. K., Thompson, J. S., Dunn, G. H., Phaneuf, R. A., Gregory, D. C., and Smith, A. C. H., *Phys. Rev. Letters* **66**, 157-60 (1991).
15. Bell, E. W., Guo, X. Q., Forand, J. L., Rinn, K., Swenson, D. R., Thompson, J. S., Bannister, M. E., Gregory, D. C., Phaneuf, R. A., Smith, A. C. H., Müller, A., Timmer, C. A., Wåhlin, E. K., DePaola, B. D., and Belić, D. S., *Phys. Rev. A* **49**, 4585-96 (1994).
16. Wallbank, B., Djurić, Woitke, O., Dunn, G. H., Smith, A. C. H., Bannister, M. E., *Phys. Rev. A* **56**, 3714-8 (1997).
17. Greenwood, J. B., Smith, S. J., and Chutjian, A., electronic aperture, unpublished results.
18. Bernius, M. T., and Chutjian, A., *Rev. Sci. Instr.* **60**, 779-82 (1989); Bernius, M. T., and Chutjian, A., *ibid.* **61**, 925-7 (1990).
(19) Ballester, G. E., McGrath, M. A., Strobel, D. F., Zhu, X., Feldman, P. D., and Moos, H. W., *Icarus* **111**, 2-17 (1994).
20. Greenwood, J. B., Smith, S. J., and Chutjian, A., e-S^{2+} excitation, unpublished results.
21. Tayal, S. S., *Astrophys. J.* **481**, 550-6 (1997).
22. Luo, D., and Pradhan, A. K., *Phys. Rev. A* **41**, 165-73 (1990).
23. Lafyatis, G. P., and Kohl, J. L., *Phys. Rev. A* **36**, 59-65 (1987).
24. Greenwood, J. B., O'Neill, R. W., Hughes, I. G., and Williams, I. D., unpublished.
25. Ramsbottom, C. A., Bell, K. L., and Stafford, R. P., *At. Data Nucl. Data Tables* **63**, 57-91 (1996).
26. Cai, W., and Pradhan, A. K., *Astrophys. J. Suppl. Ser.* **88**, 329-356 (1993).
27. Tayal, S. S., Henry, R. J. W., and Nakazaki, S., *Astrophys. J.* **313**, 487-93 (1987).
28. Greenwood, J. B., and Williams, I. D., *Physica Scripta* **T73**, 108-9 (1997).
29. Joachain, C. J., *NATO Review Book* **10** (198-).
30. Manson, S. T. *Phys. Rev.* **182**, 97-103 (1969).
31. Szydlik, P. P., Kutcher, G. J., and Green, A. E. S., *Phys. Rev. A* **10**, 1623-32 (1974).
32. Turner, C. S., and Manson, S. T., to be published.

33. Liao, C., Richard, P., Grabbe, S. R., Bhalla, C. P., Zouros, T. J. M., and Hagmann, S., *Phys. Rev. A* **50**, 1328-34 (1994).
34. Liao, C., Hagmann, S., Bhalla, C. P., and Grabbe, S. R., *Physica Scripta* **T73**, 225-6 (1997).
35. Huber, B. A., Ristori, C., and Kuchler, D., *AIP Conf. Proc. Ser.* **271**, 218 (1993).
36. Huber, B. , Ristori, C., Guet, C., Küchler, D., and Johnson, W., *Phys. Rev. Lett.* **73**, 2301-3 (1994).
37. Srigengan, B., Williams, I. D., and Newell, W. R., *Phys. Rev. A* **54**, R2540-2 (1996).
38. Srigengan, B., Williams, I. D., and Newell, W. R., *J. Phys. B* **29**, L897-900 (1996).
39. Srigengan, B., Williams, I. D., and Newell, W. R., *J. Phys. B* **29**, L605-L610 (1996).
40. Johnson, W. R., and Guet, C., *Phys. Rev. A* **49**, 1041-8 (1994).
41. Greenwood, J. B., Williams, I. D., and McGuinness, P., *Phys. Rev. Lett.* **75**, 1062-5 (1995).
42. Griffin, D. C., and Pindzola, M. S., *Phys. Rev. A* **53**, 1915-8 (1996).
43. Shull, J. M., *Physica Scripta T47*, 165-70 (1993).
44. Savage, B. D., *Physica Scripta T47*, 171-5 (1993).
45. Linsky, J. L., in *Atomic and Molecular Data for Space Astronomy* (eds. P. L. Smith and W. L. Wiese) New York: Springer Verlag, 1992.
46. Kwong, V. H. S., Fang, Z., Gibbons, T. T., Parkinson, W. H., and Smith, P. L., *Astrophys. J.* **411**, 431-7 (1993).
47. Keenan, F. P., Conlon, E. S., Harris, K. M., Aggarwal, K. M., and Widing, K. G., *Astrophys. J.* **389**, 440-2 (1992).
48. Henry, R. J. W., *Physics Reports* **68** 1-91 (1981).
49. Prior, M. H., *Phys. Rev. A* **30**, 3051-6 (1984).
50. Smith, P. L., *Atomic and Molecular Data Required for Ultraviolet and Optical Astrophysics,* Cambridge: Harvard College Observatory, 1989.
51. Calamai, A. G., Han, X. F., and Parkinson, W. H., *Phys. Rev. A* **45**, 2716-22 (1992).
52. Calamai, A. G., and Johnson, C. E., *Phys. Rev. A* **42**, 5425-32 (1990).
53. Johnson, C. E., *J. Appl. Phys.* **55**, 3207-14 (1984).
54. Johnson, B. C., Smith, P. L., and Knight, R. D., *Astrophys . J.* **281**, 477-81 (1984).
55. Kwong, H. S., Johnson, B. C., Smith, P. L., and Parkinson, W. H., *Phys. Rev. A* **27**, 3040-3 (1983).
56. Church, D., *Physics Reports* **228**, 253-358 (1993).
57. Yang, L., and Church, D. A., *Phys. Rev. Lett.* **70**, 3860-3 (1993).
58. Doschek, G. A., in *Autoionization* (ed. A. Temkin) New York: Plenum, 1985.
59. Feldman, U., Doschek, G. A., and Rosenberg, F. D., *Astrophys. J.* **215**, 652-65 (1977).
60. Edlen, B., *Physica Scripta* **23**, 1079-86 (1981).
61. Fang, Z., Kwong, H. S., and Wang, J., *Phys. Rev. A* **48**, 1114-22 (1993).
62. Lennon, D. L., Dufton, P. L., Hibbert, A., and Kingston, A. E., *Astrophys. J.* **294**, 200-6 (1985).
63. Nussbaumer, H., and Storey, P. J., *Astron. Astrophys.* **96**, 91-5 (1981).
64. Hibbert, A., and Bates, D. R., *Planet. Space Sci.* **29**, 263-8 (1981).
65. Dalgarno, A., et al. *Geophys. Res. Lett.* **8**, 603-5 (1981).
66. Cowan, R. D., Hobbs, L. M., and York, D. G., *Astrophys. J.* **257**, 373-5 (1982).
67. Knight, R. D., *Phys. Rev. Lett.* **48**, 792-5 (1982).
68. Johnson *et al.*, private communication to Calamai and Johnson.
69. Calamai, A. G., and Johnson, C. E., *Phys. Rev. A* **44**, 218-22 (1991).
70. Vevby-Christensen, L., Andersen, L. H., Heber, O., Kella, D., Pedersen, H. B., Schmidt, H. T., and Zajfman, D. *Astrophys. J.* **483**, 531-40 (1997).
71. Graham, W. G., Fritsch, W., Hahn, Y., and Tanis, J. A. eds., *Recombination of Atomic Ions*, New York: Plenum Press, 1992.
72. Larsson, M., *Int. J. Mass. Spectrom. Ion Processes* **149/150**, 403-14 (1995).
73. Kella, D., Vevby-Christensen, L., Johnson, P. J., Pedersen, H. B., and Andersen, L. H. *Science* **276**, 1530-3 (1997).